Supporting Information

Mechanistic Insights into the Oxidation of Substituted Phenols *via* Hydrogen Atom Abstraction by a Cupric Superoxo Complex

Jung Yoon Lee,[†] Ryan L. Peterson,[†] Kei Ohkubo,[‡] Isaac Garcia-Bosch,[†] Richard A. Himes,[†] Julia Woertink,[§] Cathy D. Moore,[†] Edward I. Solomon,[*,§] Shunichi Fukuzumi,[*,‡] and Kenneth D. Karlin[*,†]

[†]*Department of Chemistry, Johns Hopkins University, Baltimore, Maryland 21218, United States*

[‡] *Department of Material and Life Science, Graduate School of Engineering, Osaka University, ALCA, Japan Science and Technology Agency (JST), Osaka University, Suita, Osaka 565-0871, Japan*

[§] *Department of Chemistry, Stanford University, Stanford, California 94305, United States*

E-mail : karlin@jhu.edu, fukuzumi@chem.eng.osaka-u.ac.jp, edward.solomon@stanford.edu

(a)

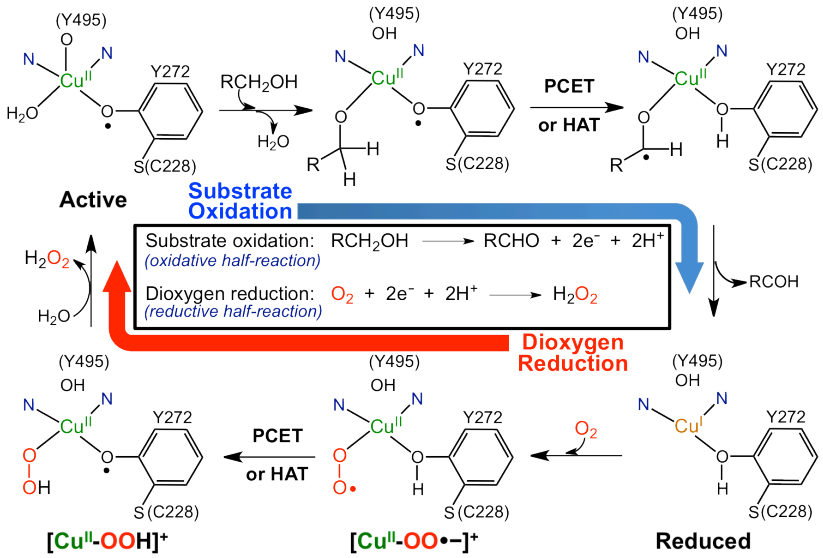

(b)

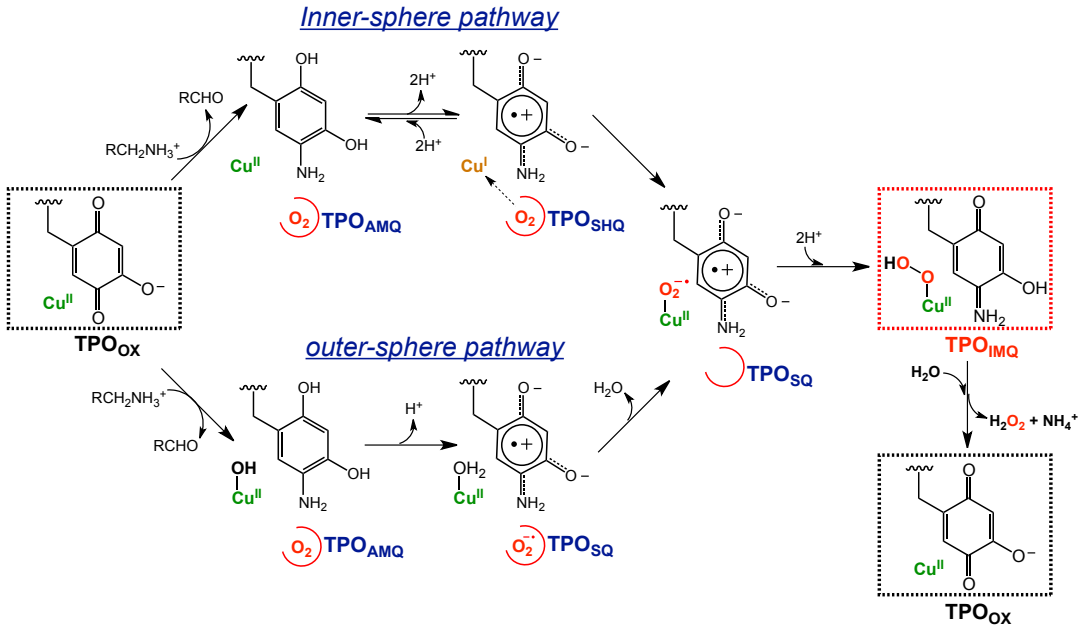

Figure S1. Proposed pathways for the primary alcohol oxidation/dioxygen reduction by galactose oxidase (GO) (a) and for copper amine oxidase (CAO) catalytic mechanism illustrating the two pathways for cofactor reoxidation (b).[a]

[a]R. L. Peterson, S. Kim, K. D. Karlin "3.07 - Copper Enzymes," In Comprehensive Inorganic Chemistry II (Second Edition); Editors-in-Chief:, J. Reedijk, K. Poeppelmeier, Ed.; Elsevier: Amsterdam, 2013; pp 149-177.

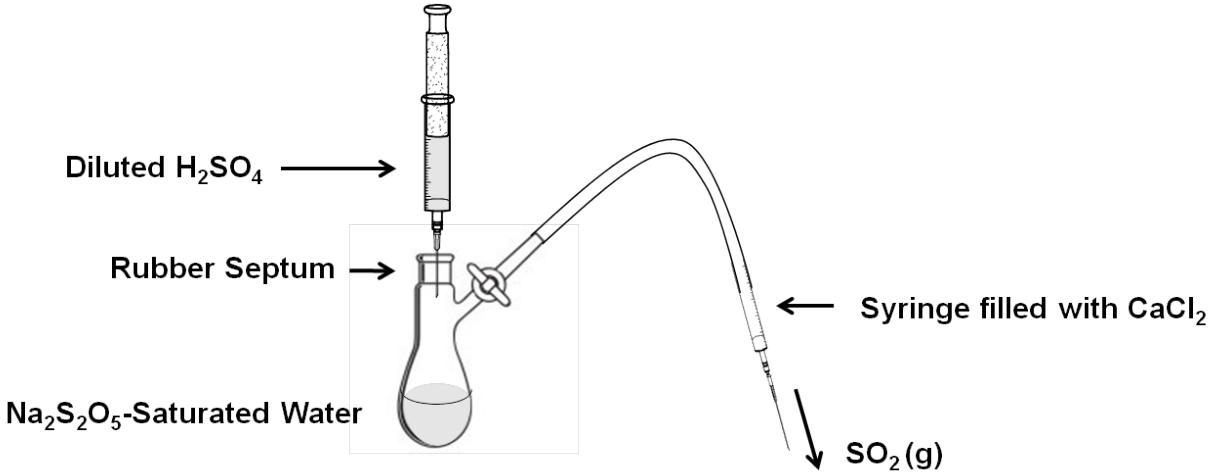

Figure S2. An apparatus setup for sulfur dioxide (SO_2, gas) generation ($H_2SO_{4\,(aq)} + Na_2S_2O_5 \rightarrow Na_2SO_4 + H_2O + 2\,SO_{2(g)}$).

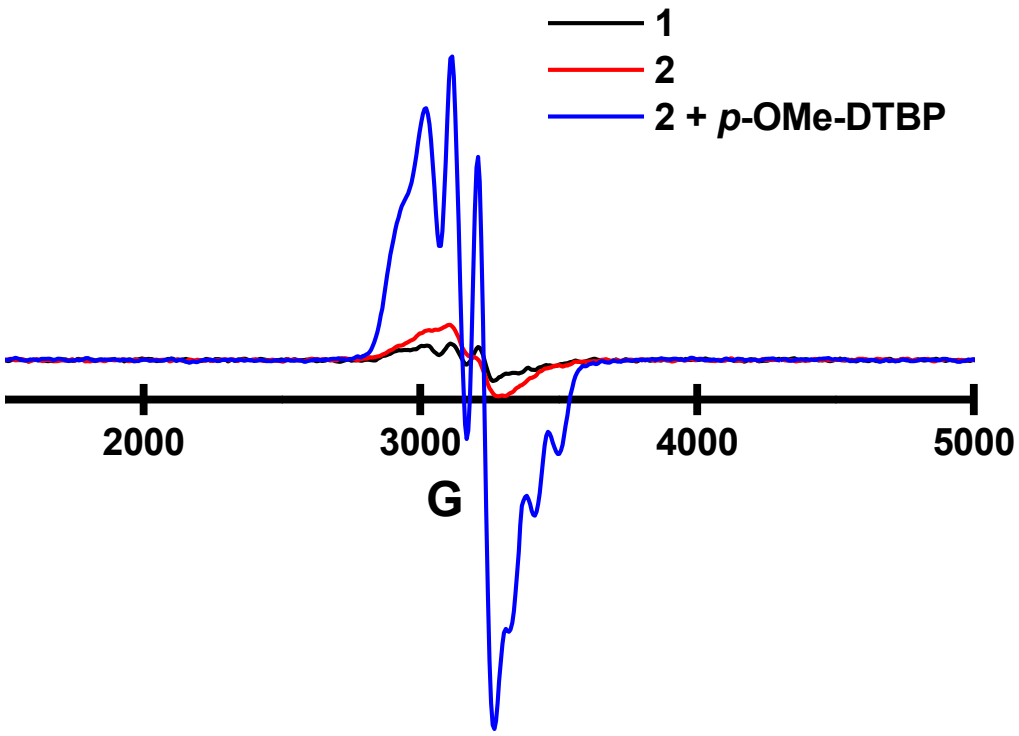

Figure S3. Low-temperature EPR spectra of [(DMM-tmpa)Cu^{I}(CO)]$B(C_6F_5)_4$ (**1**) (**black**), [(DMM-tmpa)$Cu^{II}(O_2^{\bullet-})$]$B(C_6F_5)_4$ (**2**) (**red**), and **2** + one equiv *para*-methoxy-2,6-di-*tert*-butylphenol (**blue**) (2 mM; 3X-band, ν = 9.426 GHz; acetone at 23 K): $g_{||}$ = 1.96, $A_{||}$ = 76 G, $g_{\perp}$ = 2.20, $A_{\perp}$ = 97 G. The results indicate **1** and **2** are EPR "silent", as expected, exhibiting only impurity (~ 5%) quantities of a typical copper(II) paramagnetic compound, i.e., that copper(II) complex forming by the reaction of **2** with one equiv phenol substrate. Also, see **Figure S7**.

OCH_3	
mM	s^{-1}
2.7	0.0104
4.1	0.0179
5.4	0.0234
6.8	0.0331

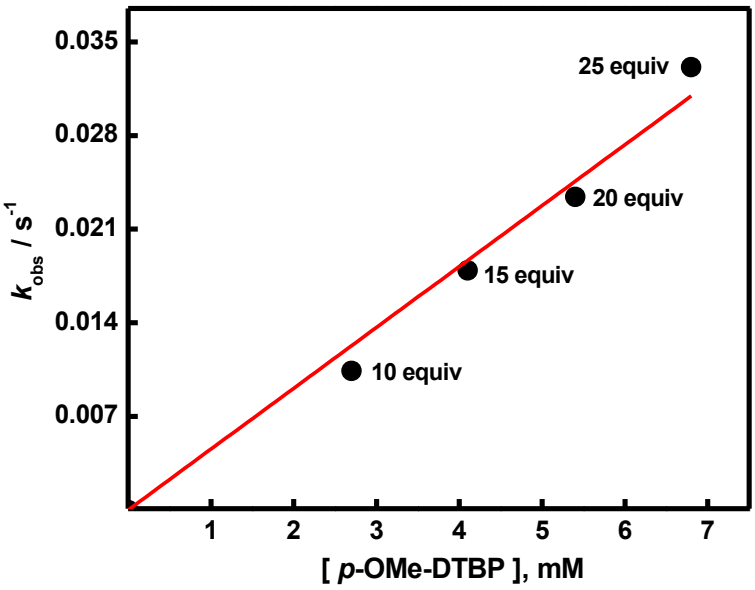

Figure S4. The table of pseudo-first-order rate constants (k_{obs}'s) from the reactions of *p*-OMe-DTBP plus $[(NMe_2\text{-tmpa})Cu^{II}(O_2^{\bullet-})]^+$ and the plot of k_{obs}'s against the concentrations of *p*-OMe-DTBP to obtain second-order-rate constant ($k_2 = 4.6\ M^{-1}s^{-1}$).

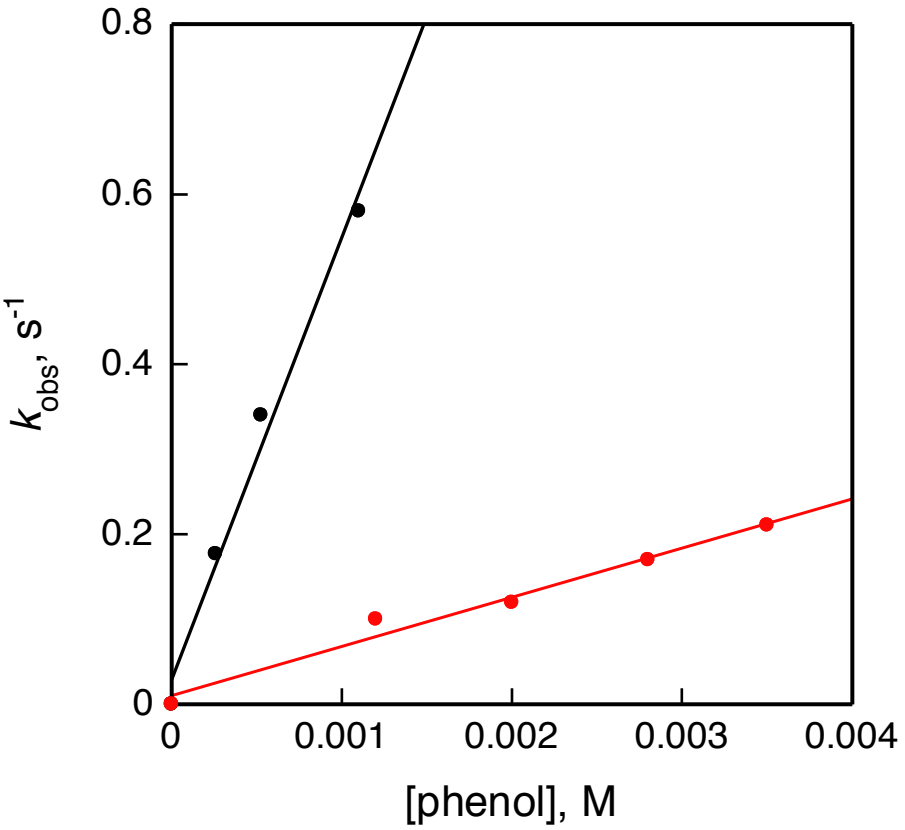

Figure S5. Plots of k_{obs}'s against the concentrations of *p*-OMe-DTBP(**black circles**) and deuterated ^{2}H-O *p*-OMe-DTBP (**red circles**) to determine second-order-rate constants and KIE (= 9.0).

	O-H					O-D					
℃	10 equiv	15 equiv	20 equiv	25 equiv	k_2	10 equiv	15 equiv	20 equiv	25 equiv	k_2	KIE
-100	0.0297	0.0425	0.058	0.0791	**11**	0.0021	0.004	0.0052	0.0063	**0.96**	**11**
-95	0.0336	0.0571	0.0784	0.0928	**14**	0.0028	0.0048	0.0069	0.0077	**1.2**	**12**
-90	0.054	0.0883	0.1248	0.1606	**23**	0.0051	0.0078	0.0112	0.0148	**2.1**	**11**
-85	0.0599	0.0984	0.1338	0.1877	**26**	0.0068	0.0099	0.0119	0.0133	**2.7**	**9.6**

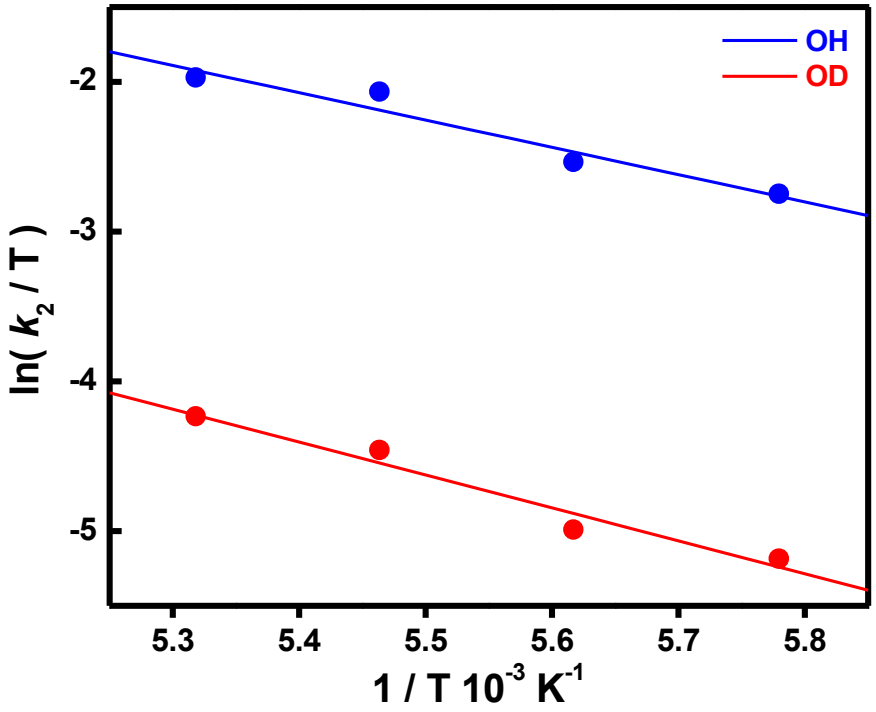

Figure S6. Table of pseudo-first-order rate constants (k_{obs}'s), second-order rate constants (k_2's) and kinetic isotope effects (KIEs) for the reactions of $[(DMM\text{-}tmpa)Cu^{II}(O_2^{\bullet-})]^+$ (**2**) and *para*-methoxy-2,6-di-*tert*-butylphenol (*p*-OMe-DTBP; H-O *vs* ^{2}H-O) in acetone over the temperature range of –100 °C ~ –85 °C (upper panel). Eyring plots of k_2's against 1/T for the oxidation of *p*-OMe-DTBP (H-O for **blue** and ^{2}H-O for **red**) to determine the reaction activation parameters (lower panel).

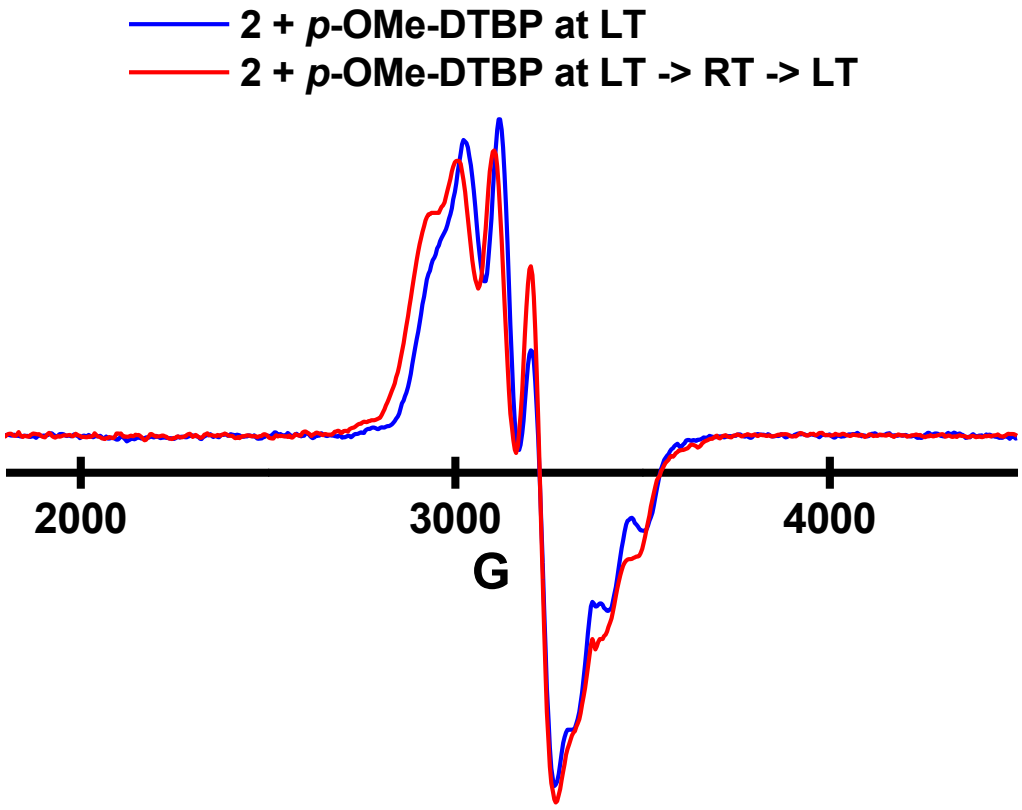

Figure S7. EPR spectra of $[(\text{DMM-tmpa})\text{Cu}^{\text{II}}(\text{O}_2^{\bullet-})]\text{B}(\text{C}_6\text{F}_5)_4$ (**2**) + one equiv *para*-methoxy-2,6-di-*tert*-butylphenol (*p*-OMe-DTBP) at low temperature (**blue**) and solution of **2** + one equiv *p*-OMe-DTBP which was warmed up to room temperature and then frozen again (**red**) (2 mM; 3X-band, ν = 9.426 GHz; acetone at 23 K). For both samples, **blue** and **red**, $g_{||}$ = 1.96, $A_{||}$ = 76 G, $g\perp$ = 2.20, A⊥ = 97 G. Thus, the **red** spectrum is representative of $[(\text{DMM-tmpa})\text{Cu}^{\text{II}}\text{-OH(H)}]^+$.

NOTE: EPR spectra observed for (***A*** ≡ ***A'***) (from mixing **2** & ArOH at –90 °C), for $[(\text{DMM-tmpa})\text{Cu}^{\text{II}}\text{-OH(H)}]^+$ (observable at RT) are indistinguishable, and further are identical to spectra of (i) $[(\text{DMM-tmpa})\text{Cu}^{\text{II}}(\text{CH}_3\text{CN})](\text{ClO}_4)_2\bullet 0.5(\text{O}(\text{CH}_2\text{CH}_3)_2)$, (ii) that species generated by reaction of $[(\text{DMM-tmpa})\text{Cu}^{\text{II}}(\text{CH}_3\text{CN})](\text{ClO}_4)_2\bullet 0.5(\text{O}(\text{CH}_2\text{CH}_3)_2)$ plus hydroxide, and (iii) that species $[(\text{DMM-tmpa})\text{Cu}^{\text{II}}(\text{OOH})]$ (**3**) generated by reaction of $[(\text{DMM-tmpa})\text{Cu}^{\text{II}}(\text{CH}_3\text{CN})](\text{ClO}_4)_2\bullet 0.5(\text{O}(\text{CH}_2\text{CH}_3)_2)$ with a small excess of $\text{H}_2\text{O}_{2(\text{aq})}/\text{Et}_3\text{N}$ or by addition of 3/2 $\text{H}_2\text{O}_{2(\text{aq})}$ to copper(I) complex **1**.

See the next page for details of the synthesis and characterization of $[(\text{DMM-tmpa})\text{Cu}^{\text{II}}(\text{CH}_3\text{CN})](\text{ClO}_4)_2 \bullet 0.5(\text{O}(\text{CH}_2\text{CH}_3)_2)$, including its X-ray structure.

Synthesis of $[(\text{DMM-tmpa})\text{Cu}^{\text{II}}(\text{CH}_3\text{CN})](\text{ClO}_4)_2 \bullet 0.5\ (\text{O}(\text{CH}_2\text{CH}_3)_2)$. In a Schlenk flask containing 100 mg of DMM-tmpa ligand and 79.7 mg of $\text{Cu}^{\text{II}}(\text{ClO}_4)_2 \bullet 6\ \text{H}_2\text{O}$ were dissolved in ~ 5 mL acetonitrile. The resulting solution was precipitated as blue solid upon addition of diethyl ether (100 mL) and crystals were obtained by vapor diffusion of diethyl ether into a solution of the complex in acetonitrile yielding 160 mg (92%) of blue crystals. **Elemental analysis:** Calculated: C (46.24), H (5.51), N (8.70); found: C (46.30), H (5.32), N (9.0).

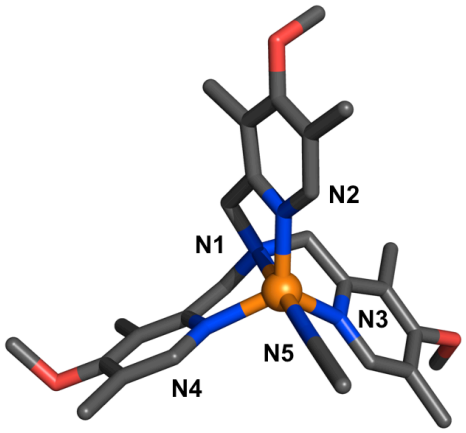

Selected Bond Lengths and Angles	
Atoms	**Bond Length(Å)**
N1-Cu1(tripod)	1.999
N2-Cu1	2.051
N3-Cu1	2.045
N4-Cu1	2.081
N5-Cu1(ACN)	1.970
	Bond Angle (°)
N1-Cu1-N5	179.15
N1-Cu1-N2	81.54
N1-Cu1-N3	81.00
N1-Cu1-N4	81.14
N2-Cu1-N5	97.83
N2-Cu1-N3	122.18
N2-Cu1-N4	117.34
N3-Cu1-N4	113.62
N3-Cu1-N5	98.87
N4-Cu1-N5	99.67

Figure S8. Left: Dicationic portion of $[(\text{DMM-tmpa})\text{Cu}^{\text{II}}(\text{CH}_3\text{CN})](\text{ClO}_4)_2$. Right: Selected bond distances and angles are given below; $\tau = 0.9495$ where a τ value = 0 would represent a perfect square-pyramid and a value of 1.0 would equal a perfect trigonal-bipyramid. See Experimental details concerning the X-ray crystallographic analysis, just below.

Experimental – $[(\text{DMM-tmpa})(\text{Cu}^{\text{II}})(\text{CH}_3\text{CN})](\text{ClO}_4)_2$

All reflection intensities were measured at 110(2) K using a KM4/Xcalibur (detector: Sapphire3) with enhance graphite-monochromated Mo *K*α radiation (λ = 0.71073 Å) under the program CrysAlisPro (Version 1.171.33.31, Oxford Diffraction Ltd., 2009). The program CrysAlisPro (Version 1.171.33.31, Oxford Diffraction Ltd., 2009) was used to refine the cell dimensions. Data reduction was done using the program CrysAlis RED (Version 1.171.33.31, Oxford Diffraction Ltd., 2009). The structure was solved with the program SHELXS-86 (Sheldrick, 2008) and was refined on F^2 with SHELXL-97 (Sheldrick, 2008). Multi-scan semi-empirical absorption corrections based on symmetry-related measurements were applied to the data using SADABS (Version 2.10). The temperature of the data collection was controlled using the system Cryojet (manufactured by Oxford Instruments). The H-atoms were placed at calculated positions using the instructions AFIX 23, AFIX 43 or AFIX 137 with isotropic displacement parameters having values 1.2 or 1.5 times *U*eq of the attached C atom.

The structure is mostly ordered. One of the two perchlorate anions is found to be disordered over three orientations, and the occupancy factors refine to 0.519(4), 0.281(5) and 0.200(3). A first refinement against F^2 was problematic because some unresolved residual electron density was found in one large void located at (0, 0.5, 0), which includes 34 electrons in a volume of 169 Å^3. This void is likely to contain a very disordered solvent molecule (likely to be diethyl ether with no full occupancy). The contribution for such solvent molecules was then taken out for the subsequent stages of the refinement using the program SQUEEZE.

Fw = 768.09*, blue block, 0.54 × 0.24 × 0.19 mm^3, triclinic, *P*-1 (no. 2), $a = 11.8100(3)$, $b = 12.4184(3)$, $c = 14.5410(3)$ Å, $\alpha = 79.3859(19)$, $\beta = 67.8701(19)$, $\gamma = 69.185(2)°$, $V = 1843.44(8)\ \text{Å}^3$, $Z = 2$, $D_x = 1.38\ \text{g cm}^{-3}$,* $\mu = 0.78\ \text{mm}^{-1}$,* abs. corr. range: 0.65–0.86. 27175 Reflections were measured up to a resolution of $(\sin\theta/\lambda)_{\text{max}} = 0.65\ \text{Å}^{-1}$. 8443 Reflections were unique ($R_{\text{int}} = 0.0397$), of which 7363 were observed [$I > 2\sigma(I)$]. 524 Parameters were refined with 349 restraints. *R*1/*wR*2 [$I > 2\sigma(I)$]: 0.0309/0.0808. *R*1/*wR*2 [all refl.]: 0.0362/0.0833. S = 1.041. Residual electron density found between −0.52 and 0.44 e Å^{-3}.

* excluding the unresolved entity contribution.

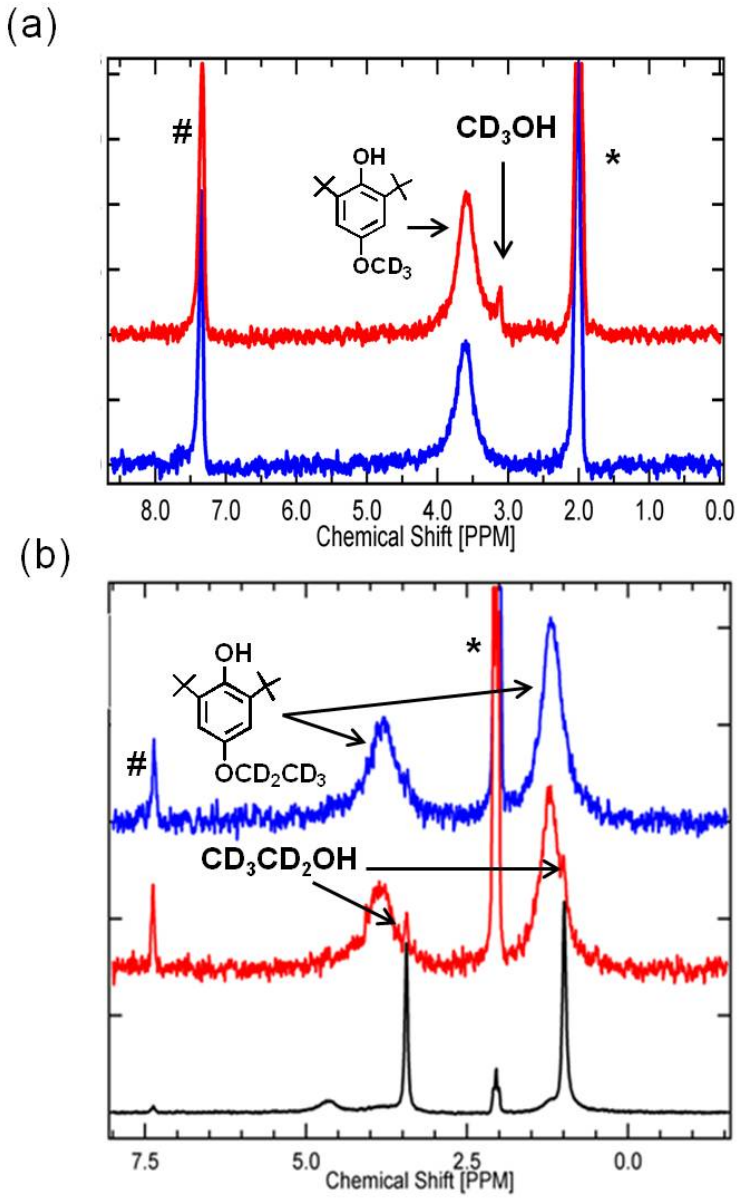

Figure S9. Low temperature ^{2}H-NMR spectra collected at –90 °C for the reaction solution of [(DMM-tmpa)Cu^{II}($O_2^{\bullet-}$)]$^{+}$ (**2**) mixed with five equiv of (a) *p*-OCD_3-DTBP and (b) *p*-OCD_2CD_3-DTBP in acetone. (a) The blue spectrum is the reaction mixture at –90 °C. The red spectrum is the reaction mixture after it is allowed to be warmed to room temperature (RT). {Note: The deuterated methanol product (CD_3OH) is only observed in the red spectrum, which forms after the reaction mixture is allowed to warm to RT.} (b) The blue spectrum is the reaction mixture at –90 °C. Displayed in the red spectrum is the NMR spectrum obtained after the reaction mixture is allowed to warm to RT. The black spectrum is the room temperature reaction mixture (blue) which was spiked with d_6-ethanol. The NMR spectral ^{2}H resonances corresponding to *p*-OCD_2CD_3-DTBP and CD_3CD_2OH are indicated with arrows, respectively. *denotes solvent, #denotes C_6H_6 used as an internal reference.

Figure S10. Pseudo-first-order plots for the reactions of $[(\text{DMM-tmpa})\text{Cu}^{\text{II}}(\text{O}_2^{\bullet-})]^+$ (**2**) and *p*-X-DTBP's to determine pseudo-first-order rate constants (k_{obs}'s). (see **Table 1** for second-order-rate constants)

(a) *p*-OCH_2CH_3-DTBP

OCH_2CH_3	
mM	s^{-1}
2.7	0.0551
4.1	0.0821
5.4	0.1233
6.8	0.1517

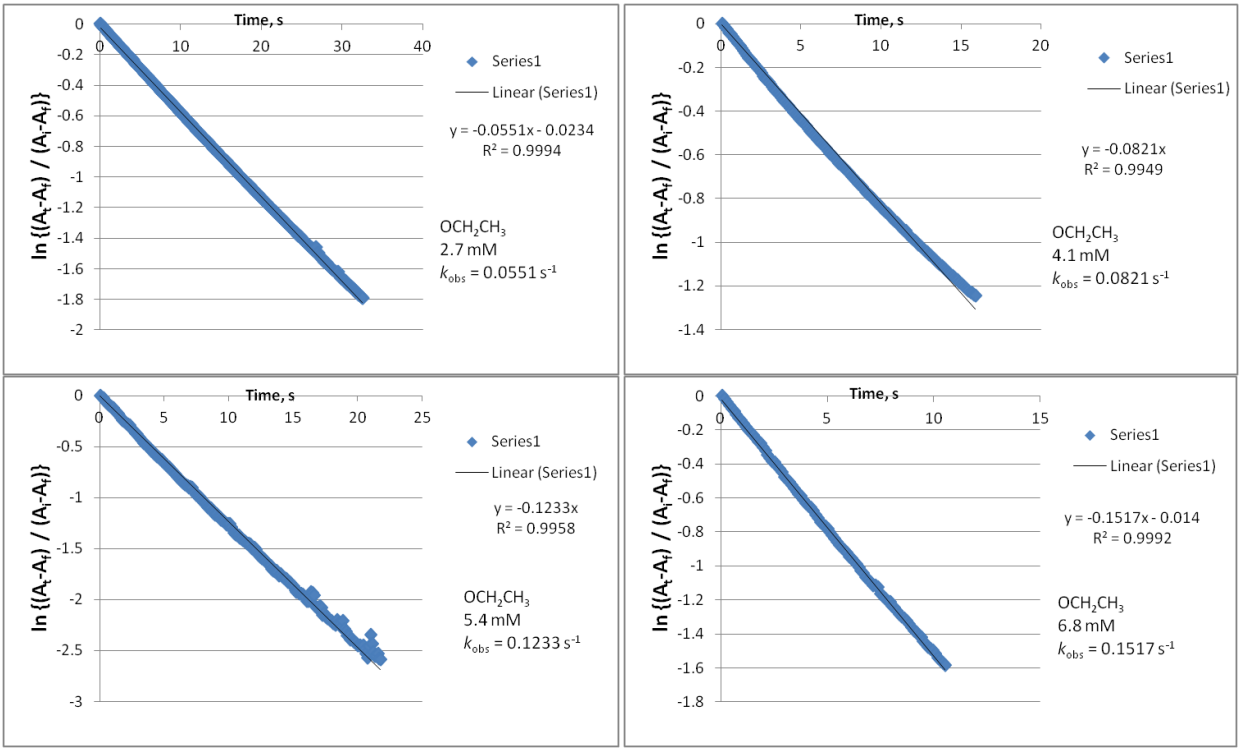

(b) *p*-OCH_3-DTBP

OCH_3	
mM	s^{-1}
2.7	0.054
4.1	0.0815
5.4	0.1248
6.8	0.1606

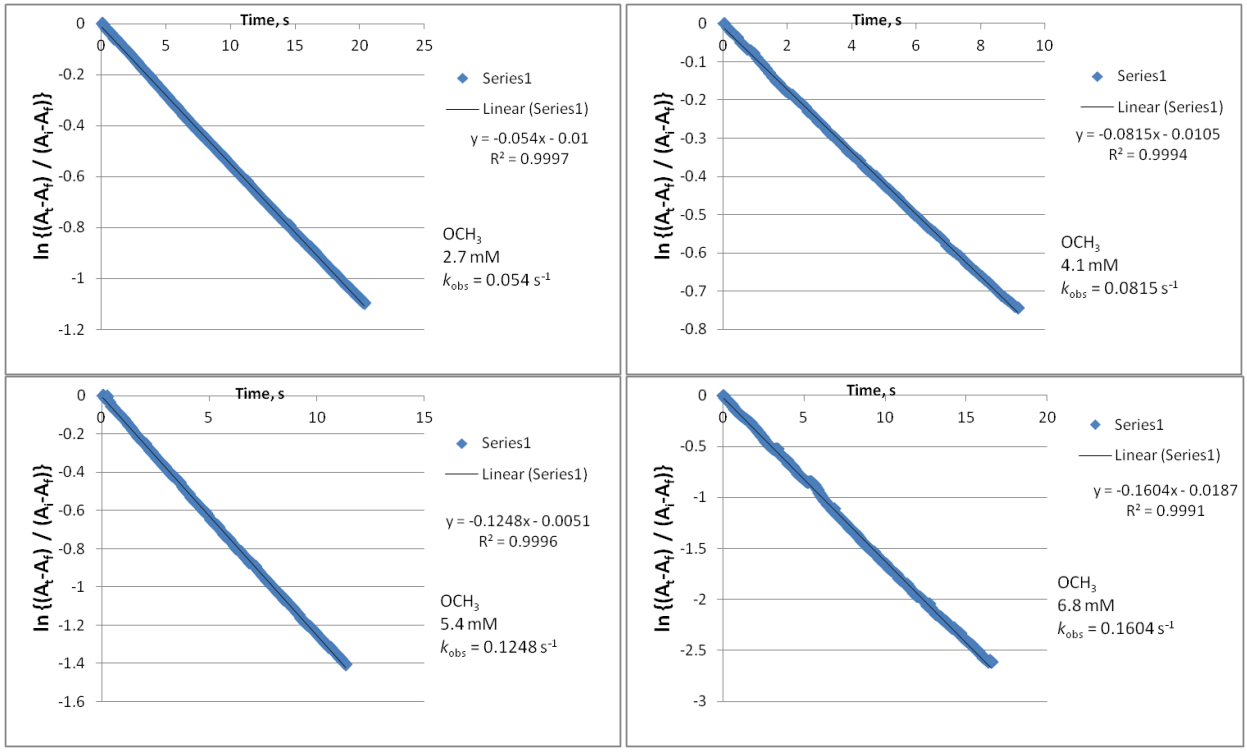

(c) *p*-OCD_3-DTBP

OCD_3	
mM	s^{-1}
3	0.0628
5	0.0948
7	0.1518
10	0.2001

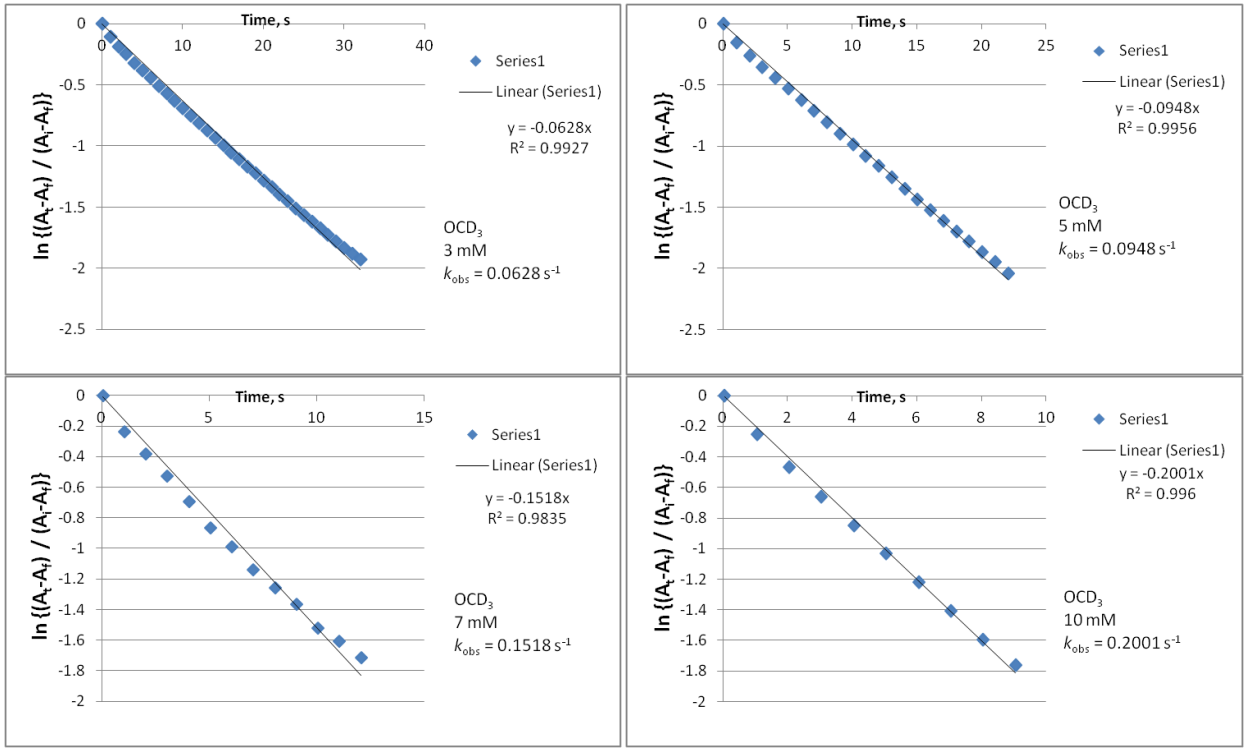

(d) *p*-OCH_3-DTBP (^{2}H-O)

OCH_3, -OD	
mM	s^{-1}
2.7	0.0054
4.1	0.0078
5.4	0.0112
6.8	0.0147

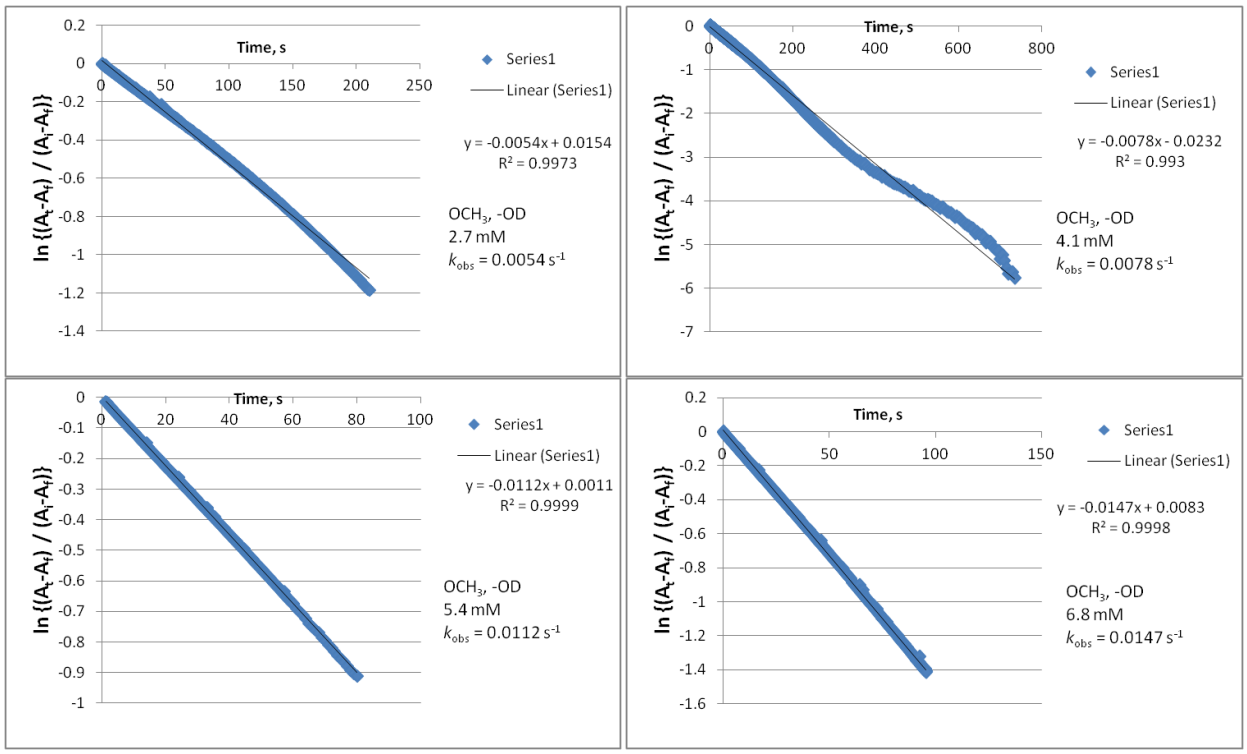

(e) *p*-OMPP-DTBP (OMPP = 2-methyl-1-phenylpropan-2-yloxy)

OMPP	
mM	s^{-1}
2.7	0.0022
4.1	0.0031
5.4	0.0041
6.8	0.0058

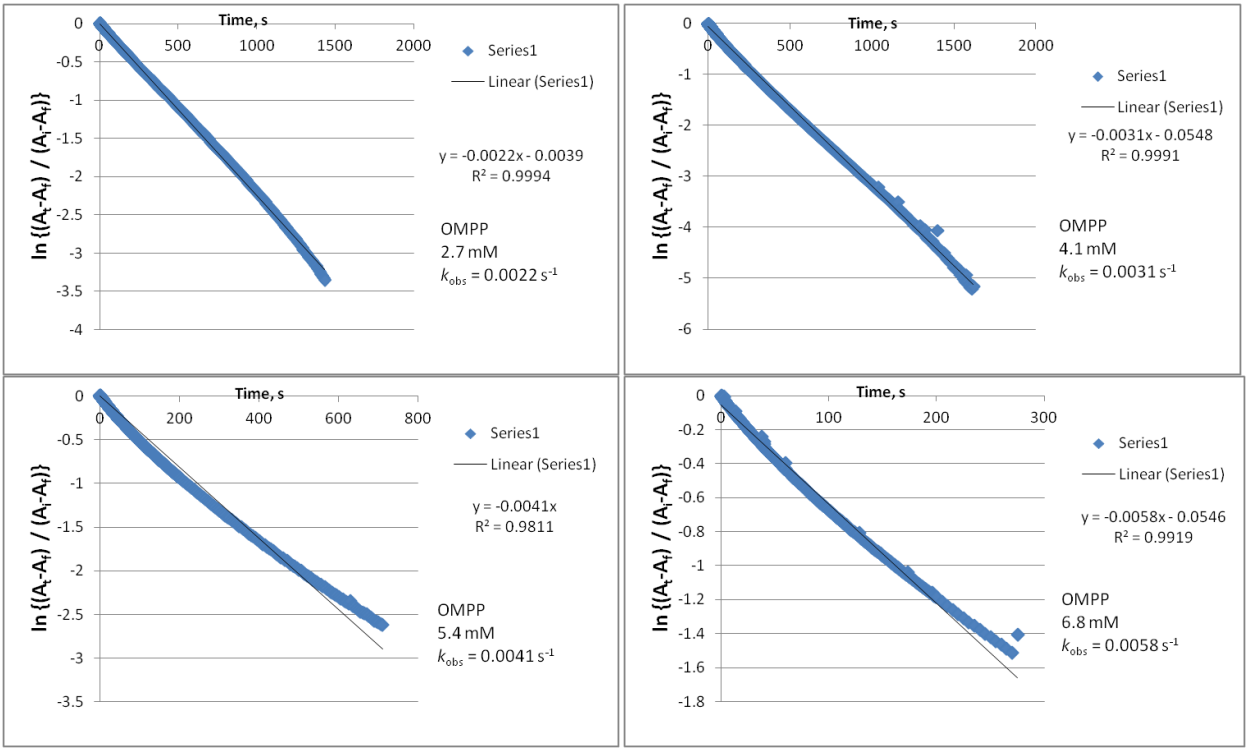

(f) *p*-OCH_2CF_3-DTBP

OCH_2CF_3	
mM	s^{-1}
3	0.0024
6	0.0051
9	0.0072
12	0.0096

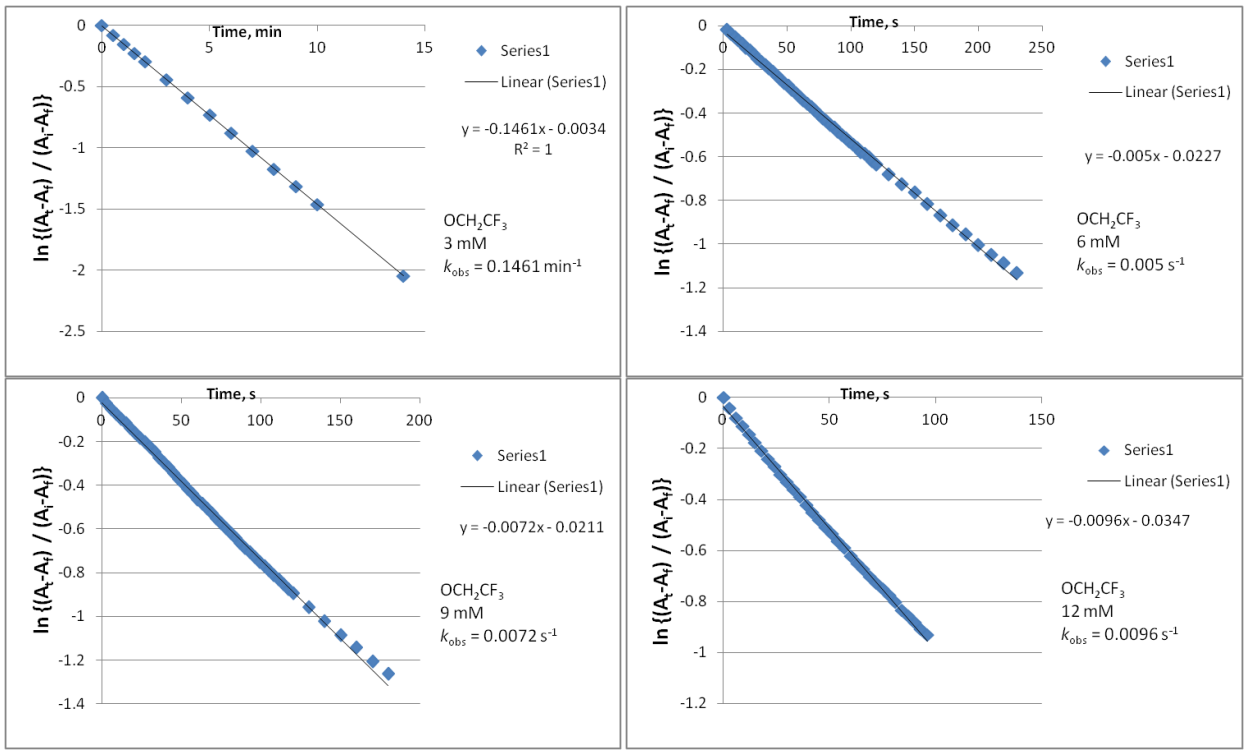

(g) *p*-CH_3-DTBP

CH_3	
mM	s^{-1}
10	4.33×10^{-4}
15	6.22×10^{-4}
20	8.07×10^{-4}
25	1.09×10^{-3}

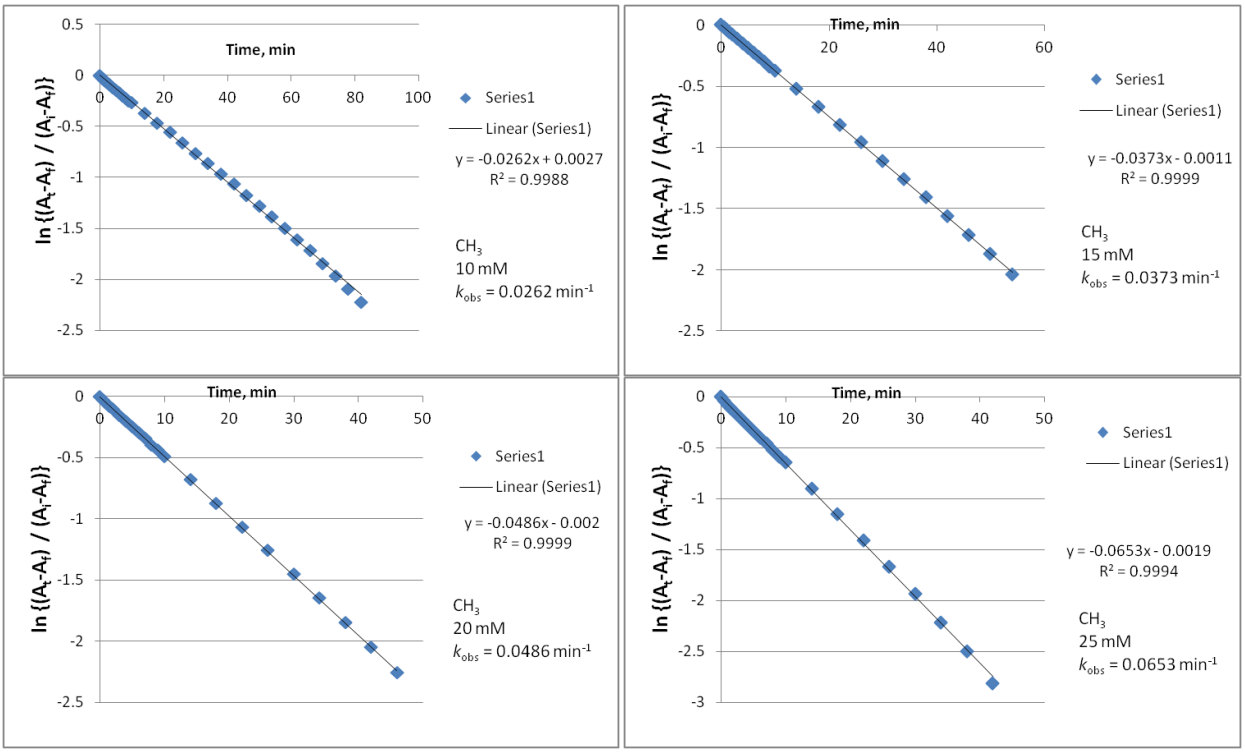

(h) *p*-CH_2CH_3-DTBP

CH_2CH_3	
mM	s^{-1}
20	5.6×10^{-4}
30	7.22×10^{-4}
40	1.03×10^{-3}
50	1.34×10^{-3}

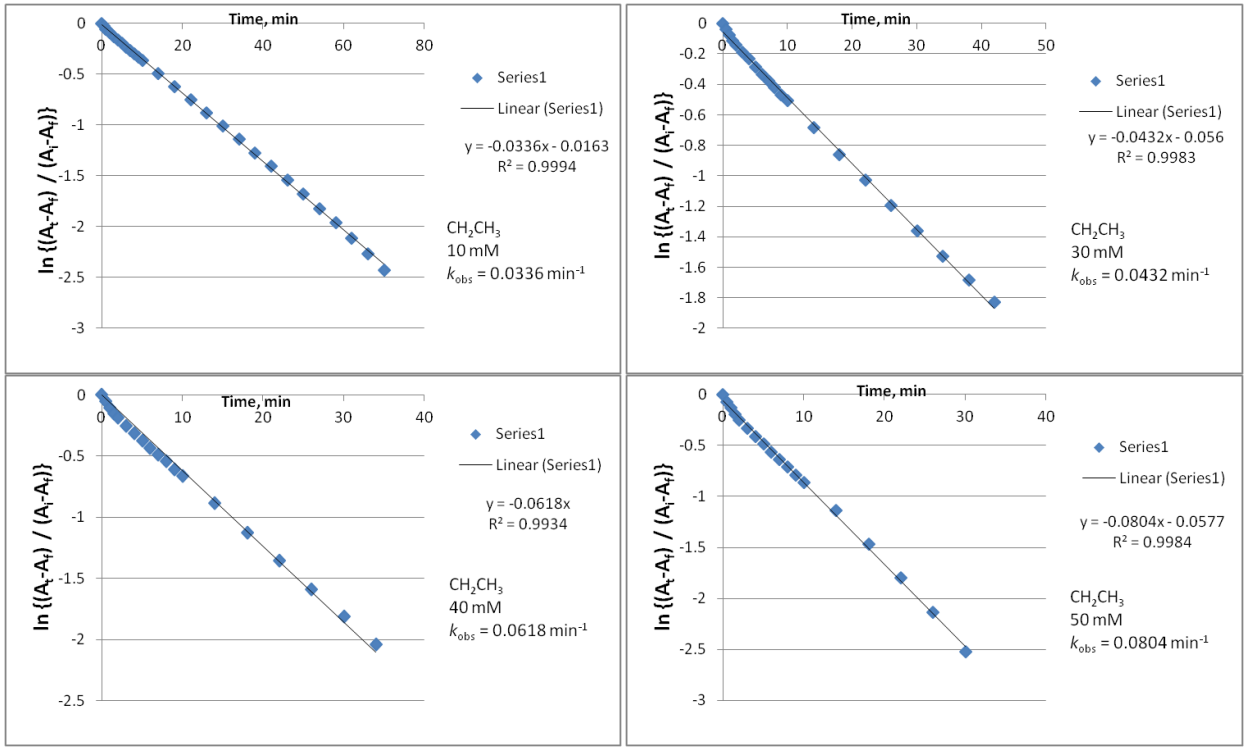

(i) *p-sec*Butyl-DTBP

sec-Butyl	
mM	s^{-1}
10	4.87×10^{-4}
30	9.38×10^{-4}
50	1.34×10^{-4}
70	1.87×10^{-4}

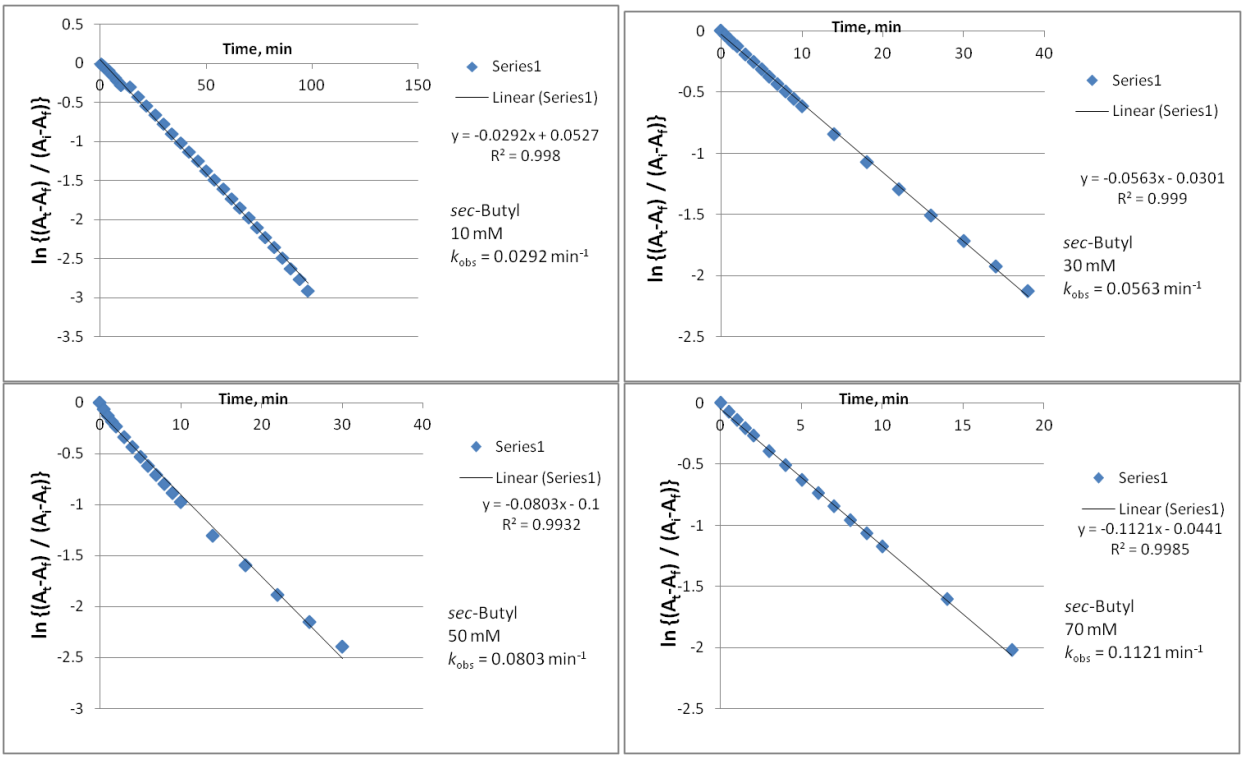

(j) *p*-CH_3-DTBP (^{2}H-O)

CH_3, -OD	
mM	s^{-1}
20	2.17×10^{-4}
25	2.5×10^{-4}
30	3.0×10^{-4}

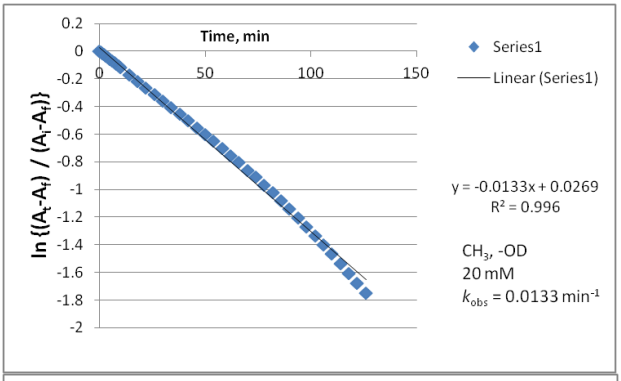

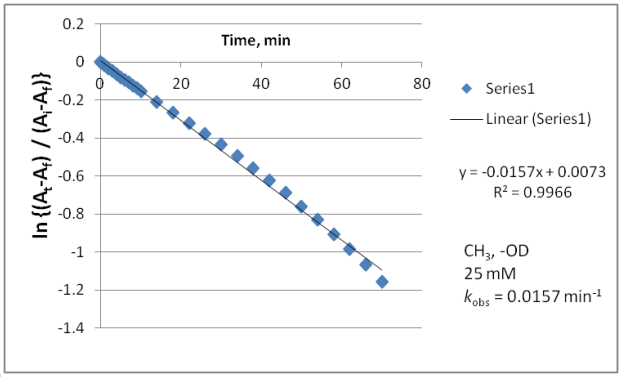

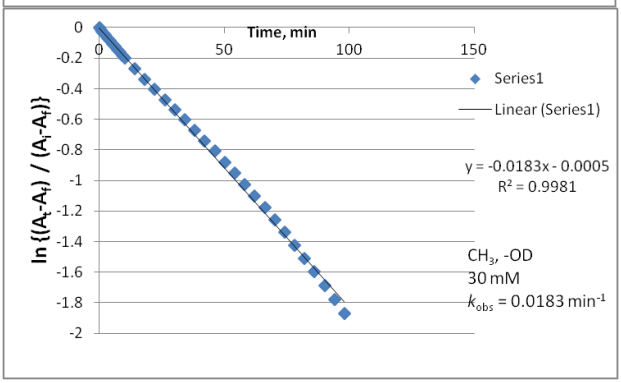

(k) *p-tert*Butyl-DTBP

tert-Butyl	
mM	s^{-1}
20	2.47×10^{-4}
25	2.82×10^{-4}
30	3.32×10^{-4}
40	4.05×10^{-4}

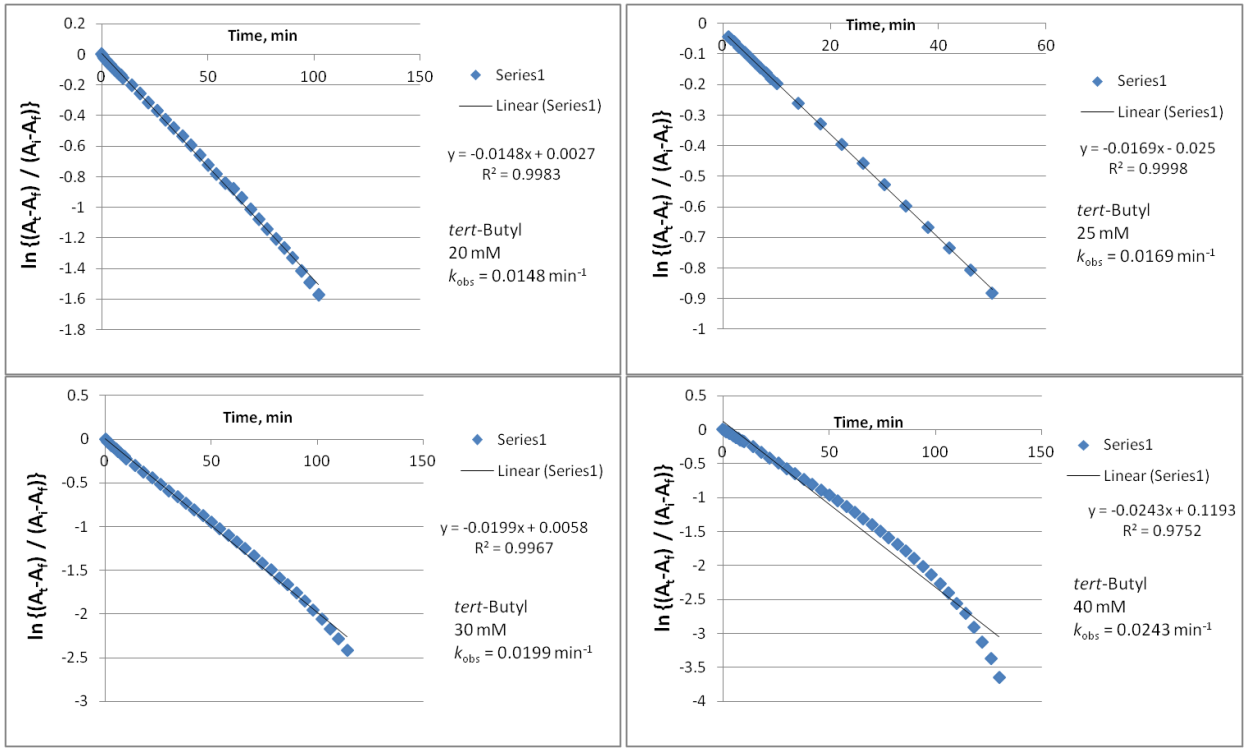

Table S1. Product Yields

	DTBQ [a]	H_2O_2 [b]	Cu complex [c]	OR / R
2 + *p*-OMe-DTBP	50 %	50 %	~ 95 %	MeOH 25 % [d]
2 + *p*-^{t}Bu-DTBP	38 %	44 %	~ 95 %	ND
2 + ^{t}BuArO·	99 %	20 ~ 30 %	~ 95 %	ND

[a] Determined by GC-MS, [b] quantified by UV-vis spectroscopy, [c] by EPR spectroscopy, and [d] by ^{2}H-NMR

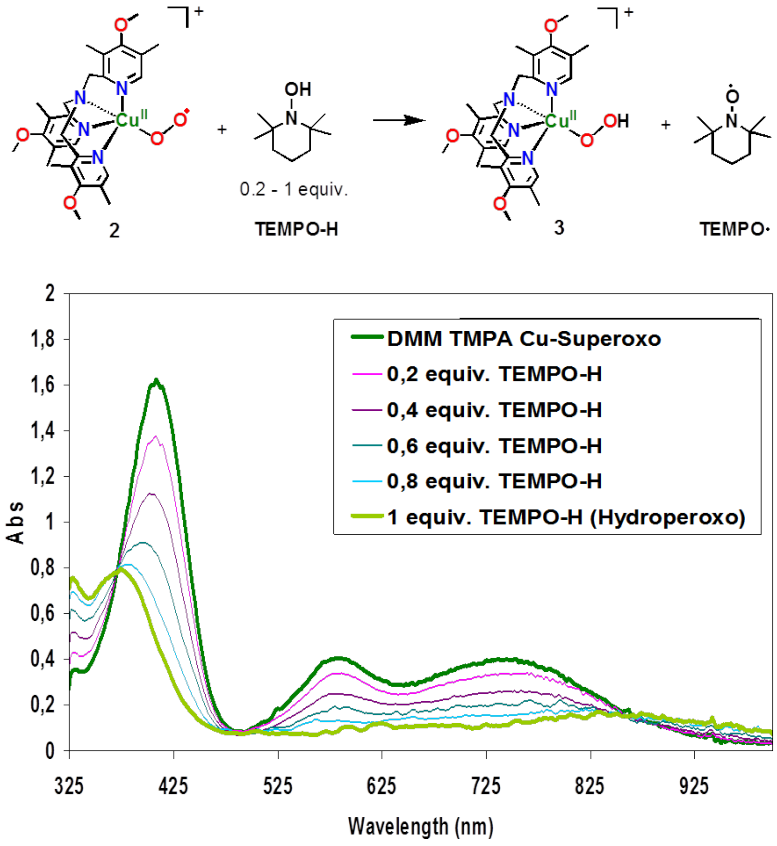

Figure S11. UV-vis spectral changes of the titration of $[(DMM\text{-}tmpa)Cu^{II}(O_2^{\bullet-})]B(C_6F_5)_4$ (**2**) 0.4 mM acetone solution with 0.2 ~ 1 equiv. TEMPO-H at 183 K affording new species presumed to be $[(DMM\text{-}tmpa)Cu^{II}(OOH)]$ (**3**) (λ_{max} = 374 nm, ε = 2000 $M^{-1}\,cm^{-1}$).

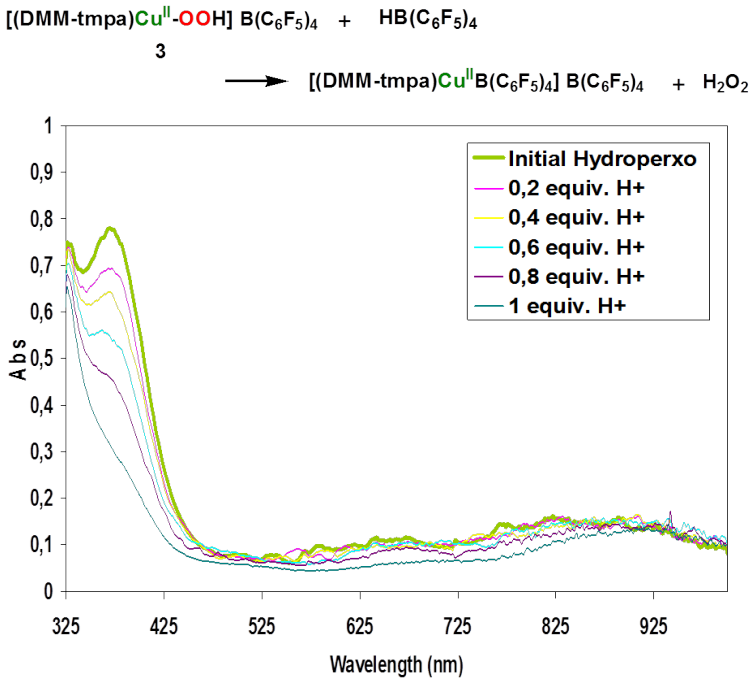

Figure S12. UV-vis spectral changes of 0.4 mM $[(DMM\text{-}tmpa)Cu^{II}(OOH)]B(C_6F_5)_4$ (**3**) acetone solution (which was generated from **2** + 0.2 ~ 1 equiv. TEMPO-H; **Figure S12**) with $H[B(C_6F_5)_4]$ acid titration.

Experimental

Quantification of H_2O_2 formed

In order to quantify hydrogen peroxide formed from the titration of the $[(DMM\text{-}tmpa)Cu^{II}(OOH)]^+$ (**3**) with acid, the following reaction was used:

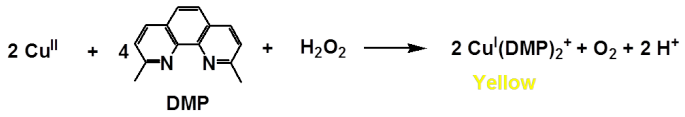

Hydrogen peroxide is an efficient reagent for the reduction of Cu(II)-2,9-dimethyl-1,10-phenanthroline (DMP) to Cu(I) species which has yellow color and exhibits specific absorption band (λ_{max} = ~460 nm).[b]

To 3 ml of reaction solution, 1 ml of 4 mM $Cu^{II}(ClO_4)_2$ solution and 1 ml of 8 mM DMP solution were added. The absorption obtained was compared to H_2O_2 standard and the yield was 40 %.

[b] Florence, T. M.; Stauber, J. L.; Mann, K. J. *J. Inorg. Biochem.* **1985**, *24*, 243-254.

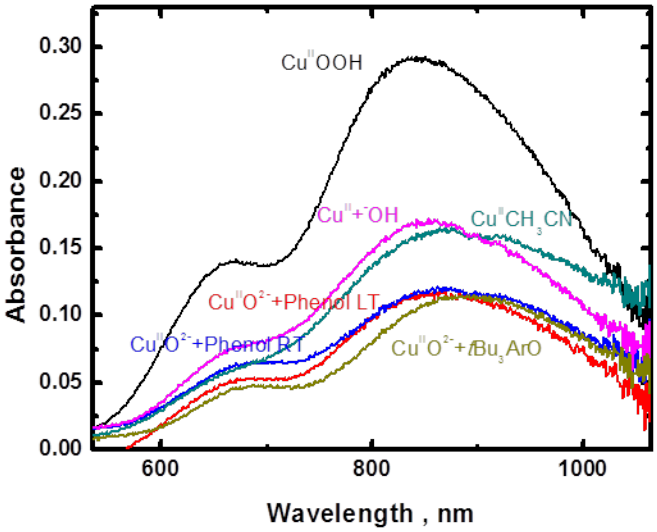

Figure S13. UV-vis spectra and *d-d* band comparison of possible Cu(II) products in acetone; (a) [(DMM-tmpa)$Cu^{II}(O_2^{\cdot-})$]$B(C_6F_5)_4$ (**2**) + phenol at low temperature (LT), (b) warmed up solution of **2** + phenol, (c) [(DMM-tmpa)$Cu^{II}(OOH)]^+$ (**3**) (LT), (d) [(DMM-tmpa)$Cu^{II}(CH_3CN)](ClO_4)_2$ at RT, (e) [(DMM-tmpa)$Cu^{II}(CH_3CN)](ClO_4)_2$ + $^tBu_4OH$ at RT, and (f) **2** + $^tBu_3ArO\cdot$ after warming to RT. We can conclude that the reactions of superoxo complex **2** with phenols lead to a $[Cu(OH)]^+$ product. EPR matching also leads to the same conclusion.

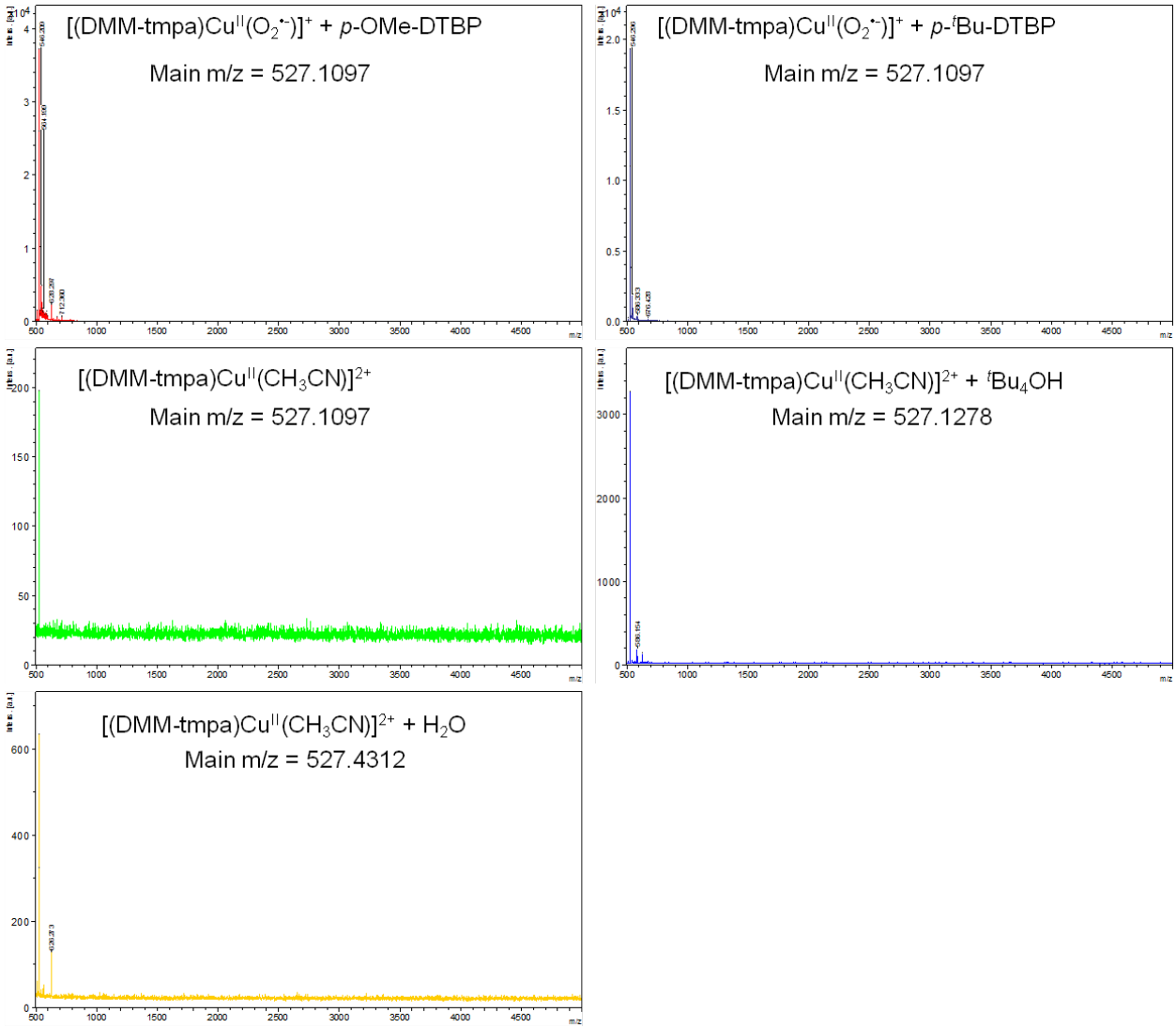

Figure S14. MALDI-TOF spectra of possible Cu(II) products; warmed up solution of [(DMM-tmpa)Cu^{II}(O$_2^{\bullet-}$)]$^+$ + phenol, [(DMM-tmpa)Cu^{II}(CH$_3$CN)]$^{2+}$, [(DMM-tmpa)Cu^{II}(CH$_3$CN)]$^{2+}$ + ^{t}Bu$_4$OH, and [(DMM-tmpa)Cu^{II}(CH$_3$CN)]$^{2+}$ + H$_2$O. Under all conditions the [(DMM-tmpa)Cu^{I}]$^+$ is the major or only species observed and so mass spectrometry, either ESI-MS or MALDI-TOF-MS cannot distinguish between [(DMM-tmpa)Cu^{II}-X]$^+$ complexes.

Experimental

MALDI-TOF mass spectra were obtained using a Bruker AutoFlex III MALDI-TOF mass spectrometer. Samples were prepared in acetone and deposites on the target plate in the absence of any added matrix.